Title

Rapid fluorescence lifetime estimation with modified phasor approach and Laguerre deconvolution: a comparative study

Permalink

https://escholarship.org/uc/item/0cg7w2hh

Journal

Methods and Applications in Fluorescence, 5(3)

ISSN

2050-6120

Authors

Fereidouni, Farzad
Gorpas, Dimitris
Ma, Dinglong
et al.

Publication Date

2017

DOI

10.1088/2050-6120/aa7b62

Peer reviewed

Rapid fluorescence lifetime estimation with modified phasor approach and Laguerre deconvolution: a comparative study

Farzad Fereidouni[1], **Dimitris Gorpas**[2], **Dinglong Ma**[2], **Hussain Fatakdawala**[2], and **Laura Marcu**[2]

[1]Department of Pathology and laboratory medicine, 4400 V Street, CA 95817

[2]Department of Biomedical Engineering, University of California, Davis, 451 Health Science Dr, Davis, CA 95616 USA

Abstract

Fluorescence lifetime imaging has been shown to serve as a valuable tool for interrogating and diagnosis of biological tissue at a mesoscopic level. The ability to analyze fluorescence decay curves to extract lifetime values in real-time is crucial for clinical translation and applications such as tumor margin delineation or intracoronary imaging of atherosclerotic plaques. In this work, we compare the performance of two popular non-parametric (fit-free) methods for determining lifetime values from fluorescence decays in real-time –the Phasor approach and Laguerre deconvolution. We demonstrate results from simulated and experimental data to compare the accuracy and speed of both methods and their dependence on noise and model parameters.

Keywords

Fluorescence; Lifetime imaging; Laguerre deconvolution; phasor analysis

1.Introduction

The excited state Lifetime of fluorescence molecules offers valuable information for diagnosis and characterization of biological tissues and it provides a sensitive contrast mechanism for imaging. Similar to fluorescence spectrum, the excited state decay curve offers important information on the state of a fluorescence molecule and its interaction with its immediate environment including PH [1], oxygen saturation [2], calcium concentration [3, 4] and it has been used for studying molecular interactions through Forster resonance energy transfer [5], and more recently is extensively evaluated as a means of tissue diagnostics [6, 7].

1.1 Fluorescence Lifetime as a contrast mechanism

Endogenous fluorophores are commonly studied for purposes of tissue diagnostics. This includes amino acids, structural units of proteins, collagen and elastin that impart

---

Correspondence to: Laura Marcu.

Conflicting interests: The authors have declared that no conflicting interests exist.

mechanical and elastic strength to tissues, NADH and FAD that regulate cell metabolism and porphyrins that are a by-product of metabolism. These fluorophores have been studied to characterize and distinguish healthy and diseased tissue *in vivo* and *ex vivo* [8]. As a result, fluorescence based imaging techniques have the potential to quantitate biochemical and structural changes in tissue in relation to clinical diagnosis [8]. The intensity and spectral distribution of fluorescence emission are commonly used in optical measurements but are often plagued with broad spectrally overlapping emission spectra,, tissue heterogeneity and dependence on excitation-collection geometry. Time-resolved fluorescence methods, on the other hand, consider the decay characteristics of the fluorescence emission providing better differentiation between fluorophores with overlapping spectra. Since the decay characteristics are an intrinsic property of a fluorophore, lifetime values are independent of instrumentation and the excitation-collection geometry. This makes lifetime measurements robust and reproducible from multiple measurements (with varying experimental setups), making it a promising tool for clinical translation. Our previous work has explored the application of fluorescence lifetime imaging (FLIm) for oral carcinoma detection [9], atherosclerotic plaque assessment [10] and characterization of engineered tissues [11]. More recently we have also reported the ability to measure lifetime from tissue and to augment white-light video frames in real-time [12, 13]. Quantification of emission spectrum and lifetime is performed through different analysis tools. While the spectrum can take different inconsistent shapes and normally is identified with its peak position and width, the decay curve of fluorescence which exhibits a single exponential behavior can be identified with a single number which is the characteristic of exponential decay time or its lifetime.

1.2 FLIM Data analysis

Compared to intensity-based measurements, lifetime measurements require not only more complex hardware and electronics but also more advanced data analysis. The latter arises from the fact that the recorded fluorescence intensity decay curve is convolved with the instrument response function (IRF) which can present with a temporal width comparable to the lifetime of the decay curve. Extracting the pure decay curve from the convolved curve has been the subject of many studies. One straight forward approach is to truncate the decay curve with an offset after the IRF peak intensity and employ a multi-exponential model to extract lifetime values [2]. This assumes that the width of the IRF is significantly smaller than the measured lifetime. This has been shown to be a simple and straightforward method in many studies employing excitation source with significantly shorter pulse duration (i.e. femtosecond or few ps range) when compared to the expected fluorescence lifetime[14]. Nevertheless, ignoring the beginning of the decay curve to circumvent this problem costs the loss of the information of shorter lifetimes components and losing the large part of the signal which occurs at the earlier part of the decay curve. Different algorithms including non-linear least squares [15], Laplace transformation [16], method of moments [17], maximum likelihood [18], Laguerre series expansion [19] and phasor approach [20] have been developed to overcome this problem. Some of these methods are computationally intensive and are limited by their low speed which makes them less favorable for real-time utilizations.

In contrast with controllable environments (i.e. cell imaging or dye solutions), in more complex systems, like the case of biological tissues, the type and/or the number of the intrinsic fluorophores is rarely known *a priori*. Moreover, in such a system the decay mechanism cannot be fully described by a multi-exponential model. Thus, instead of assuming a system with discrete fluorophores, a model described by a range of exponential decays with a range of lifetime values is needed [2, 21]. In this regard, implementation of non-parametric mathematical models that do not require *a priori* knowledge of the underlying decay characteristics or any information regarding the number of the fluorophores is beneficial.

The phasor approach and Laguerre deconvolution method have become popular recently for analysis of fluorescence lifetime data [15, 19, 20, 22]. In this paper, we demonstrate the implementation and comparison of these two non-parametric (fit-free) methods for rapid lifetime estimation of fluorescence decay curves. The phasor approach is a graphical method that has been developed for analysis of lifetime and spectral images and it offers a graphical representation of the recorded decay curve on a 2D plot. Accounting for the instrument response effect is simply performed by a separate reference measurement considering the fact that deconvolution can be performed with a simple division in the Fourier domain. Usually, only the first harmonics is used for estimation of the lifetime as the higher harmonics have lower signal to noise ratios[23, 24]. There are other multifrequency approaches which use higher harmonics to extract multiple lifetime components and their fractional intensities but they are either slower or less accurate for average lifetime estimation[25–27]. One of the interesting features of the phasor approach is the reciprocal property [28]. The phasors of decay curves with various lifetimes fall on a unique positions inside the reference semicircle and this provides a mechanism for basic segmentation.

The Laguerre method involves expanding the fluorescence decay onto an ordered set of discrete-time Laguerre basis functions. These functions form an orthonormal set and the measured fluorescence (a convolution of the instrument response and the fluorescence decay) can be parameterized using the Laguerre expansion coefficients. Hence the estimation of these coefficients allows the deconvolution of the decay from the instrument response. A fast constrained least-squares Laguerre deconvolution technique has been previously reported [15], where mathematical constraints are applied to ensure that the recovered decay is positive, monotonically decreasing, convex and asymptotically approaching zero.

In this study, we evaluate these two methods with both simulated and experimental data obtained using a pulse-sampling time-domain time-resolved fluorescence technique [29, 30] and for distinct conditions (i.e. sampling rate, total duration of signal recording and signal to noise ratio). In addition, we evaluate the background effect when fiber-optics are used to excite and collect fluorescence from tissue and the sensitivity of the two methods to different levels of additive noise and background. Background signal is an inevitable part of tissue measurements, which is generated by experimental conditions including the fiber autofluorescence. The goal of this current study is to closely inspect the performance of these two methods for their accuracy, speed and in particular for *in-situ* tissue evaluation.

2.Methods and Materials

2.1. The phasor approach

The phasor method is a fit-free method that has been shown to be a powerful tool for the analysis of fluorescence lifetime [20, 22, 31] or spectral images [28, 32, 33]. This method provides a graphical representation of the fluorescence decay that is comparatively simpler than other existing methods but needs prior calibration on well characterized samples in order to correct for the IRF effect and to obtain quantitative results [4]. Briefly, the real and imaginary parts of the Fourier transformation of the fluorescence decay curve or fluorescence emission spectrum are used as coordinates in the phasor plot.

The generated plot and the image are correlated; every point in the phasor plot can be traced back to pixels with the same property in the image. Moreover, every decay curve is mapped onto a unique position in the phasor plot and the position of the phasor determines the lifetime. A region of interest in the phasor diagram can be back projected to the pixels correlated with the selected phasor points. This results in fast and convenient image segmentation.

The application of this approach to time-domain data with different time resolution settings and acquisition periods has been shown before [22, 34]. This theoretical frame work can be applied to different settings including sampling rate or total detection window. The general phasor semi-circle is expressed by:

$$R(\tau, n) = \frac{1}{\cos\left(\frac{\pi}{N}\right) - \sin\left(\frac{\pi}{N}\right)\coth\left(\frac{T}{2N\tau}\right)j}, \quad (1)$$

where N is the number of time-sampling points of the decay curve, T is the total acquisition period, and τ is the lifetime. R is a complex number and the reference semicircle is generated by drawing the imaginary part of R versus its real part. Figure 1, shows the modified reference semicircle adopted for different numbers of sampling points and the same acquisition period for a lifetime range from $\tau/T = 0.01$ to $\tau/T = 5$. As the lifetime increases the phasor moves on the semicircle from right to left. When $N \to \infty$, R converges to the standard phasor curve [22]:

$$R(\tau, n) = \frac{1}{1 - jn\frac{2\pi}{T}\tau}. \quad (2)$$

The average lifetime can be estimated by the following equation [14]:

$$\tau = \frac{T}{2N\coth^{-1}\left(\frac{S}{G}\cot\left(\frac{\pi}{N}\right)\right)}, \quad (3)$$

where S is the imaginary and G the real part of the phasor. However, when the sampling number is large, $N \to \infty$, this equation is reduced to its standard format[23]. The effect of the IRF on the fluorescence decay can be simply considered by either a rotation of the phasors over a fixed angle obtained from a reference measurement on a dye with a known lifetime or by direct measurement of the IRF.

2.2. Laguerre Deconvolution

Estimation of lifetime based on Laguerre deconvolution is another model-free method currently commonly used to analyze the fluorescence decay data [30, 35, 36]. This method is based on the expansion of the fluorescence decay curve on a set of Laguerre basis of functions (LBF) [19]. This approach was found to provide significant advantages over the more traditional methods when applied to tissue characterization.

In general, the measured fluorescence decay intensity $F(t)$ is a convolution of the true signal $h(t)$ and the instrument impulse response function $x(t)$. Through application of a constrained least-square deconvolution process, the fluorescence transient signal, $\hat{h}(k)$, can be approximated. In discrete time, for N equal sampling time points, $t_i = i\delta t_{\ i=0....,N-1}$ and sampling interval δt gives,

$$F(k) = \sum_{i=0}^{k} x(k-i) \cdot h(i), \quad (4)$$

where $k = 0,...,N-1$. $h(k)$ is expanded on to a set of discrete ordered LBF, b_l such that,

$$h(k) = \sum_{l=0}^{L-1} c_l b_l(k;\alpha), \quad (5)$$

where L and α are the basis parameters and c_l is the lth expansion coefficient. The lth discrete time LBF is defined as

$$b_l(k;\alpha) = \alpha^{(k-l)/2}(1-\alpha)^{1/2} \sum_{l=0}^{i} (-1)^i \binom{k}{i}\binom{l}{i}\alpha^{l-i}(1-\alpha)^i \quad (6)$$

For $l = 0,..., L-1$ and $0 < \alpha < 1$. Since LBF forms an orthonormal set,

$$b_l^T b_{l'} = \delta_{ll'}, \quad (7)$$

where $b_l = [b_l(0;\alpha),...,b_l(N-1;\alpha)]^T$ and $\delta_{ll'}$ is the Kronecker delta function. For a set of L basis functions we have $B = [b_0, b_1,..., b_{L-1}]$ such that $B^T B = I$. Here, I is the identity matrix. Consequently, $\hat{h}(k)$ is defined by the Laguerre expansion coefficients $c = [c_0, c_1,..., c_{L-1}]^T$. These coefficients can be estimated using a fast constrained least-square

deconvolution technique [37]. The constraints described by Liu *et al.* [15] ensure that $\hat{h}(k)$ is positive, monotonically decreasing, strictly convex and asymptotically approaches zero, representing physical characteristics of fluorescence decay signals. The average lifetime can then be calculated from $\hat{h}(k)$ as follows,

$$\tau_{avg} = \frac{\delta t \sum_k k \cdot h(k)}{\sum_k h(k)}. \quad (8)$$

The Laguerre deconvolution method, unlike multi-exponential models, involves a linear optimization scheme with a unique solution and eliminates the need for *a priori* knowledge of the number of decay components that can be arbitrary for a complex fluorescing system such as tissue. In addition, the method provides a faster way of computing lifetimes that would be important for on-line data analysis as needed in a clinical setting.

2.3 Simulated data

2.3 Simulated data—To study the noise effect on the lifetime estimation, simulated mono-exponential decay curves convolved with experimental IRF, were generated. The lifetime values of these decays ranged from 0.5 ns to 15 ns with steps of 500 ps. White Gaussian noise and Poisson noise model were applied to the simulated decay curves separately. The former approximates the noise of a system using pulse sampling technique. The latter represents the noise of a shot-noise limited photon counting system. Although more comprehensive noise model of the pulse sampling technique is available [38], system dependent parameters are required to provide an accurate description. Here we chose white Gaussian noise as a valid simplification. Different levels of noise were introduced to the simulated decay curves resulting into SNR (signal-to-noise ratios) ranging from 10 dB to 60 dB. For white Gaussian noise, the SNR is defined as $SNR = 10\log_{10}\left(\frac{1}{\sigma^2}\right)$. ($\sigma^2$ is the noise variance, while the peak amplitude is normalized to 1.) For Poisson noise, the SNR is given by $SNR = 10\log_{10}\left(\sqrt{N}\right)$. (N is the number photons.) Next, we analyzed the two sets of simulated data using both phasor and Laguerre methods. (α=0.9181 was used for Laguerre method.)

When using fiber-optics for fluorescence excitation and collection, the acquired transient signals are often contaminated by a background signal due to the fiber autofluorescence. For studying the effect of background on lifetime estimation from measured decay curves, we considered four cases: background present, background removed, and two cases where the background was partially removed. To remove the background, the mean value of the separately measured background signal and decay curves were first determined and then their ratio was used to normalize the background. The normalized background was subtracted from the decay curve with 3 different scaling factors of 2, 1 and 0.5. Four sets of synthetic data with bi-exponential behavior were generated for the cases mentioned above and analyzed with both phasor and Laguerre methods. The lifetimes of two components were randomly distributed between 0.5 ns to 10 ns and their contribution to the total decay curve was also randomly chosen. An experimental IRF, recorded separately was used to

perform the convolution and finally a measured background was added to all the decay curves and noise was added. We note that the direct current (DC) background effect is not evaluated here. The pulse-sampling technique used and therefore, this study is independent from ambient illumination since the pre-amplifier used is AC coupled that filters out any DC components of the acquired signals. Thus, the DC background effect is minimal. Moreover, the treatment for DC background effect for the phasor approach has been considered previously by Reinhart et al. [39] using photon counting instruments.

2.4 Experimental data

Experimental data was generated using fluorescence dye solutions and a piece of fresh tissue. Time-resolved fluorescence measurements were performed in a C120 solution (Exciton, Coumarin 440, 5 mM in Ethanol) using a multi-spectral time-resolved fluorescence spectroscopy device developed by our group and reported previously [40]. In brief, fluorescence was induced by a 355 nm pulsed diode laser (HE1060-10uJ-SP, frequency tripled, Fianium, UK), spectrally resolved by a custom-made wavelength selection module (WSM) into four different bands of central wavelength/bandwidth 390/40 nm (channel 1), 452/45 nm (channel 2), 545/50 nm (channel 3) and 629/53 nm (channel 4), detected by a single micro-channel plate photomultiplier (MCP-PMT) and finally time-resolved by a fast digitizer (National Instruments, PXIe 5185, 3 GHz bandwidth, 12.5 GHz sampling rate). For the case of C120 only channel 2 was used, as this fluorophore presents an emission peak at 430 nm. The fluorescence decay of the Coumarin solution was recorded with different levels of SNR by changing the PMT anode voltage and by averaging the decays.

Raster scanning measurement on fresh tissue (purchased from a supermarket) was implemented over a 25×25 mm^2 region with scanning speed 2 mm/s and vertical step 0.5 mm. Fluorescence lifetime data was collected from different tissue types (i.e. bone, fat, muscle). Background is removed from the experimental data as explained before.

3.Results and discussion

3.1 Simulated data

3.1.1 Effect of SNR on lifetime estimation accuracy—In this section, we demonstrate the behavior of the two methods using both Gaussian and Poissonian statistics. Figure 2 (a) shows the phasor plot for the decay curve with lifetime of 10 ns and different ranges of SNR generated using Gaussian noise. The phasor of a mono-exponential decay curve falls on the global semicircle and as it is shown on figure 2 (a), a decay curve with high SNR generates a phasor point on the semicircle. By decreasing the SNR, the points in the phasor deviate from the semicircle, are shifted towards the origin and present more spread.

Two decay curves are shown for extreme SNRs in figure 2 (a) and it also demonstrates how the lifetimes are estimated after generating the phasor plot. For curves with low SNR, the measured phase shows a larger deviation in comparison to the phase of a decay curve with higher SNR. This inaccuracy in phase measurement results in inaccuracy of the estimated

lifetimes. Figure 2 (b) depicts the histogram for the lifetime estimation of a decay curve with given value of 10 ns calculated with both phasor and Laguerre methods. The relative error for a lifetime of 10ns is computed as 0.0045 and 0.036 from phasor and Laguerre methods respectively. However, the relative standard deviation is calculated as 0.157 and 0.074 from phasor and Laguerre. The relative error is a measure of accuracy (how far is the maximum of the histogram from the real value) and the relative standard deviation is a measure of precision which reflects the width of the histogram calculated from lifetime estimation using the two techniques. While the phasor shows a better accuracy, the precision for the Laguerre method is higher. The histogram from the phasor method is broader but the maximum is closer to the real value. On the other hand, the histogram from Laguerre method is sharper but its peak position is far from the real value. Figure 2 (c) and figure 2 (d) depict the relative error and relative standard deviation, respectively. For shorter lifetime values, the error for lifetime estimation was large (0.8 for lifetime of 1ns) for both methods. This is due to the lower number of sampling points of decay curves with shorter lifetimes. This error levels out at the central region of the graph for both methods but it increases again due to the truncation of the decay curves. Truncation occurs because of the limited total acquisition period of decay curves which prevents complete recording of the decays. This trend is more pronounced for the estimated lifetimes from the Laguerre method. The results for the effect of Gaussian noise on the accuracy of lifetime estimation are shown in Figure 3 for three different lifetimes of 1 ns, 5 ns and 10 ns. The plots show the relative error as a function of SNR. Phasor shows more vulnerability to higher Gaussian noise. As the noise level increases the average of estimated lifetime deviates from the real values towards smaller values [14]. This trend is less significant for the calculated lifetimes from Laguerre approach but it also deviates towards smaller lifetime values. As the noise level increases, approximation of lifetime values is based on earlier temporal locations of the decay curve, biasing the results towards smaller lifetime values (i.e. faster decays). By increasing the SNR, the estimated lifetime from the phasor approach is recovered rapidly towards true values and in comparison, the lifetimes calculated by Laguerre method provide more accurate estimation. In comparison with the Laguerre method, the phasor approach provides higher speed and accuracy but the precision is lower.

Analysis of 5000 decay curves using the phasor approach on a standard personal computer (PC) takes less than 0.6 seconds. The same amount of data is analyzed with Laguerre within 8.5 seconds. However, the susceptibility of the phasor method to noise is higher when compared to Laguerre. As shown in figure 3, the relative error for estimated lifetime values decreases rapidly with larger SNR values using the phasor method. This improves both precision and accuracy of lifetime estimation. With larger SNR available, the phasor method provides a better dynamic range. However, Laguerre shows lower accuracy for shorter lifetime values even with very high SNRs.

The simulation is repeated for mono-exponential behavior using Poissonian noise (Figure 4). In contrast with the case of Gaussian noise, as the SNR decreases the phasor cloud spreads around a given point along the phasor global semicircle. Figure 4 (b) shows the shape of the phasor cloud for a decay curve with lifetime of 10ns and different levels of SNR. Also, in comparison to the case when only Gaussian noise is present, the precision of both methods increases. This becomes obvious when the relative standard deviations (figures 4(c) and

4(d)) are compared to figures 2(c) and 2(d). The accuracy follows the same trend as before and Laguerre shows more susceptibility to truncation of the decay curves as the relative error is larger for longer lifetimes.

Figure 5, shows the relative error as a function of SNR for three different lifetime values 1ns, 5ns and 10ns. In contrast to the case with Gaussian noise, the phasor method shows lower relative error (higher accuracy) for all lifetime ranges in comparison to the Laguerre method. However, both methods show lower relative errors with Poissonian noise. Also, in comparison to Gaussian noise, the estimated lifetime values converge faster to the real values as the SNR increases.

3.1.2 Background artefact removal—Figure 6 shows the phasor plots for all the approaches of background removal. Interestingly, the removal of background can be easily observed in the phasor plot. As expected, the elongation of the phasor points from the top of the semicircle towards the (1,0) coordinate indicates the presence of a range of lifetime values in the data set. By subtracting a wrongly scaled background signal from the decay curves, the phasor clouds move towards inside or outside the phasor reference semicircle (figure 6 (a), (b)). The results are summarized in Table 1 for average of relative errors. The phasor shows more susceptibility to incorrect background subtraction. Also, figure 6 (e) shows the separately measured background profile.

3.2 Experimental Data

3.2.1 Effect of SNR on lifetime estimation accuracy—In this section, we analyze and compare the experimental data for different levels of SNR by variation of amplification voltage of the PMT and also averaging of decay curves. Figure 7 shows the phasor plot for 4 different states. The variation of SNR is reflected on the size of the phasor cloud. [R6:] By using ~400 nJ pulse energy for excitation, and efficient Coumarin dye [41], we estimate the detected fluorescence photons are more than 10,000. According to the filtered Poisson process with additive Gaussian noise model for pulse sampling technique [38], low gain voltage and small number of averaging result in Gaussian noise dominated measurement; increasing the gain voltage and number of averaging will both increase the overall SNR, while shifting the noise characteristic toward the comprehensive noise model with both Gaussian and Poissonian components.Figure 7 (a) shows the phasor plot for a case where the measurement is performed with PMT anode voltage set to 1600V. Because both Gaussian and Poissonian noise are present, the elongation of the phasor cloud is not towards the origin of the phasor plot, as one might expect from the case where only Gaussian noise is present. By changing the voltage to higher values (i.e. 1800 V) the signal amplitude increases while the Gaussian noise remained the same. This results in a narrow elongation of the phasor cloud shape, which can be realized by comparing figurers 7(a) to 7(b). By changing the averaging size from 4 to 16 and to 64 both Poissonian and Gaussian noise decrease. This leads to further reduction of the total size of the phasor cloud as previously reported [32] and ultimately improves the accuracy of the lifetime estimation. When comparing the two methods, it was observed that although they show slightly different means over the entire data set they show a similar trend with regards to the standard deviation. Figure 8 summarizes the results for 4 different voltages and averaging settings on a box plot.

Comparing the experimental data to simulated results, a few observations were consistent. Under low SNR conditions (1650V, 4AVG and 1800V, 4AVG) the mean lifetimes from Laguerre method (2.32 ns and 2.27 ns) are longer than the values from Phasor approach (2.31 ns and 2.24 ns); the standard deviations are also slightly higher for Laguerre method (0.31 ns and 0.12 ns) compared to Phasor approach (0.28 ns and 0.10 ns). This reflects the increased relative error and relative standard deviation of Laguerre method compared to Phasor approach at 2 ns point.

3.2.2 Imaging biological tissues—Figure 9 (a) and Figure 9 (b) depict imaging results from the tissue sample analyzed using both methods where the lifetime maps are overlaid on the white light images. Both methods have led to similar lifetime values. As demonstrated by the phasor plot (Figure 9 (c)), a range of different lifetime values exist in the imaged field. It is clearly realized due to the elongation of the phasor cloud indicating that multiple biological components with different lifetimes have been imaged. Figure 9 (d) shows a zoomed region and also two regions of interest indicated by white circles.

By finding the corresponding pixels to the selected regions in the phasor plot, it is possible to map the selected region of interests back to the image. This is due to the reciprocal property of the phasor method and it is explained elsewhere [20]. The small region on the top of the phasor corresponds to fat in the tissue and the larger region of interest is selected, highlights the muscle and bone marrow. Although the average lifetime of the fat and bone are similar on the lifetime maps (~6.5 ns), applying the reciprocal property of the phasor enables us to distinguish between these two types of the tissue. This is a great feature of the phasor approach which facilitates the separation of different tissues based on their decay curve and not the estimated average lifetime values. Thus, it provides a higher contrast for tissues with similar average lifetime values but different lifetime components.

4. Conclusion

The major challenge in the analysis of fluorescence lifetime data is the deconvolution of the instrument response function from the measured fluorescence decay curve to extract the intrinsic fluorescence decay dynamics and to quantify the lifetime value(s) of a fluorescent molecule. This procedure has been performed traditionally with iterative deconvolution methods using multi-exponential functions [42]. This methodology is slow, requires intensive computation, and is also biased with initial inputs.

Among many methods developed for analysis of fluorescence decay curves, fit-free algorithms like phasor and Laguerre deconvolution provide faster solution for analysis. This paper provides the first comparison of the performance of these two methods and evaluates their potential for online (real-time) characterization of tissues properties.

One of the interesting features of phasor plots is the graphical representation of the data. The level of SNR of the data can be easily inferred from the shape of the phasor cloud. Larger SNR, shows smaller cloud and lower SNR make the phasor cloud spread around the average lifetime phasor vector. Also with the background analysis, where the decay curves are single exponential, it is very easy to spot the proper background treatment; as the phasor cloud

moves outside or inside the reference semicircle with background subtraction which was not scaled correctly.

The lifetime approximation through a set of Laguerre basis functions is a robust non-parametric model that has been used to study the fluorescence dynamics from biological tissues [30, 35, 36]. Application of this model does not require any *a priori* knowledge of the underlying decay characteristics or any information regarding the number of the fluorophores. By relying on expansion basis sets, this model is based on more simplified mathematical expressions and can be solved through more efficient numerical approaches [15].

While the phasor method shows a more accurate estimation of the lifetime values, the Laguerre based analysis resulted in a higher precision. However, the accuracy level of this method depends on the initial parameters ($\alpha=0.9181$)]used for expansion and it is a function of the lifetime distribution in the decay curve. We observed that the Laguerre analysis is susceptible to the truncation and sampling of the data as it shows a larger error with shorter and longer lifetimes. On the other hand, Laguerre provides additional information about the decay mechanism through the expansion coefficients which can be used for more detailed analysis of the fluorescence decay. One of the strong points of Laguerre method is that it is less biased with the SNR and it provides lifetime estimation with higher precision for decay curves with very low SNR.

The trends of relative error and standard deviation are consistent between the two noise mechanisms used in this study (Gaussian and Poissonian). Although the trends of relative standard deviation were consistent for both methods in both noise configurations, quantitative conclusions can hardly be drawn due to different definitions of SNR for Gaussian and Poissonian noise. The mechanisms of Gaussian and Poissonian noises on the results of the phasor and Laguerre based analysis methods are different, while the Laguerre based analysis is optimized for Gaussian noise and the phasor performs better with Poissonian noise. Such a difference was indicated by the observation that the phasor clouds changed distribution for Gaussian and Poissonian noises. In experimental systems using pulse sampling or time-gating techniques, noise of both Gaussian and Poissonian characteristics can be present, which require characterization of the instrumental variability in lifetime estimation.

In conclusion, we studied two fit-free algorithms for real-time identification and diagnosis of tissues. The evaluation of the phasor method for graphical segmentation and quantification of different components in the image could be the subject for future studies.

Acknowledgments

References

1. Hight MR, Nolting DD, McKinley ET, Lander AD, Wyatt SK, Gonyea M, Zhao P, Manning HC. Multispectral fluorescence imaging to assess pH in biological specimens. Journal of biomedical optics. 2011; 16 016007-016007-016007.

2. Lakowicz JR. Principles of fluorescence spectroscopy Springer Science & Business Media; 2013

3. Agronskaia AV, Tertoolen L, Gerritsen HC. Fast fluorescence lifetime imaging of calcium in living cells. Journal of Biomedical Optics. 2004; 9:1230–1237. [PubMed: 15568944]

4. Celli A, Sanchez S, Behne M, Hazlett T, Gratton E, Mauro T. The epidermal Ca 2+ gradient: measurement using the phasor representation of fluorescent lifetime imaging. Biophysical journal. 2010; 98:911–921. [PubMed: 20197045]

5. Fereidouni F, Blab GA, Gerritsen HC. Phasor based analysis of FRET images recorded using spectrally resolved lifetime imaging. Methods and Applications in Fluorescence. 2014; 2:035001. [PubMed: 29148469]

6. Sun Y, Hatami N, Yee M, Phipps J, Elson DS, Gorin F, Schrot RJ, Marcu L. Fluorescence lifetime imaging microscopy for brain tumor image-guided surgery. Journal of biomedical optics. 2010; 15 056022-056022-056025.

7. Sun Y, Phipps JE, Meier J, Hatami N, Poirier B, Elson DS, Farwell DG, Marcu L. Endoscopic fluorescence lifetime imaging for in vivo intraoperative diagnosis of oral carcinoma. Microscopy and Microanalysis. 2013; 19:791–798. [PubMed: 23702007]

8. Berezin MY, Achilefu S. Fluorescence lifetime measurements and biological imaging. Chemical reviews. 2010; 110:2641–2684. [PubMed: 20356094]

9. Fatakdawala H, Poti S, Zhou F, Sun Y, Bec J, Liu J, Yankelevich DR, Tinling SP, Gandour-Edwards RF, Farwell DG. Multimodal in vivo imaging of oral cancer using fluorescence lifetime, photoacoustic and ultrasound techniques. Biomedical optics express. 2013; 4:1724–1741. [PubMed: 24049693]

10. Fatakdawala H, Gorpas D, Bishop JW, Bec J, Ma D, Southard JA, Margulies KB, Marcu L. Fluorescence Lifetime Imaging Combined with Conventional Intravascular Ultrasound for Enhanced Assessment of Atherosclerotic Plaques: an Ex Vivo Study in Human Coronary Arteries. Journal of cardiovascular translational research. 2015:1–11. [PubMed: 25583535]

11. Fatakdawala H, Griffiths LG, Humphrey S, Marcu L. Time-resolved fluorescence spectroscopy and ultrasound backscatter microscopy for nondestructive evaluation of vascular grafts. Journal of biomedical optics. 2014; 19:080503–080503. [PubMed: 25147960]

12. Ma D, Bec J, Gorpas D, Yankelevich D, Marcu L. Technique for real-time tissue characterization based on scanning multispectral fluorescence lifetime spectroscopy (ms-TRFS). Biomedical optics express. 2015; 6:987–1002. [PubMed: 25798320]

13. Gorpas D, Ma D, Bec J, Yankelevich D, Marcu L. Real-time visualization of tissue surface biochemical features derived from fluorescence lifetime measurements. 2016

14. Fereidouni F, Reitsma K, Gerritsen HC. High speed multispectral fluorescence lifetime imaging. Optics express. 2013; 21:11769–11782. [PubMed: 23736399]

15. Liu J, Sun Y, Qi J, Marcu L. A novel method for fast and robust estimation of fluorescence decay dynamics using constrained least-squares deconvolution with Laguerre expansion. Physics in medicine and biology. 2012; 57:843. [PubMed: 22290334]

16. Gafni A, Modlin RL, Brand L. Analysis of fluorescence decay curves by means of the Laplace transformation. Biophysical journal. 1975; 15:263. [PubMed: 1122338]

17. Esposito A, Gerritsen HC, Wouters FS. Fluorescence lifetime heterogeneity resolution in the frequency domain by lifetime moments analysis. Biophysical journal. 2005; 89:4286–4299. [PubMed: 16169974]

18. Bajzer Ž, Therneau TM, Sharp JC, Prendergast FG. Maximum likelihood method for the analysis of time-resolved fluorescence decay curves. European biophysics journal. 1991; 20:247–262.

19. Jo JA, Fang Q, Marcu L. Ultrafast method for the analysis of fluorescence lifetime imaging microscopy data based on the Laguerre expansion technique. Selected Topics in Quantum Electronics, IEEE Journal of. 2005; 11:835–845.

20. Digman MA, Caiolfa VR, Zamai M, Gratton E. The phasor approach to fluorescence lifetime imaging analysis. Biophysical journal. 2008; 94:L14–L16. [PubMed: 17981902]

21. Cubeddu R, Comelli D, D'Andrea C, Taroni P, Valentini G. Time-resolved fluorescence imaging in biology and medicine. Journal of Physics D: Applied Physics. 2002; 35:R61.

22. Fereidouni F, Esposito A, Blab G, Gerritsen H. A modified phasor approach for analyzing time-gated fluorescence lifetime images. Journal of microscopy. 2011; 244:248–258. [PubMed: 21933184]

23. Gratton E, Breusegem S, Sutin J, Ruan Q, Barry N. Fluorescence lifetime imaging for the two-photon microscope: time-domain and frequency-domain methods. Journal of biomedical optics. 2003; 8:381–390. [PubMed: 12880343]

24. Grecco HE, Roda-Navarro P, Verveer PJ. Global analysis of time correlated single photon counting FRET-FLIM data. Optics express. 2009; 17:6493–6508. [PubMed: 19365474]

25. Weber G. Resolution of the fluorescence lifetimes in a heterogeneous system by phase and modulation measurements. The Journal of Physical Chemistry. 1981; 85:949–953.

26. Squire A, Verveer PJ, Bastiaens P. Multiple frequency fluorescence lifetime imaging microscopy. Journal of Microscopy. 2000; 197:136–149. [PubMed: 10652007]

27. Esposito A, Popleteeva M, Venkitaraman AR. Maximizing the biochemical resolving power of fluorescence microscopy. PloS one. 2013; 8:e77392. [PubMed: 24204821]

28. Fereidouni F, Bader AN, Colonna A, Gerritsen HC. Phasor analysis of multiphoton spectral images distinguishes autofluorescence components of in vivo human skin. Journal of biophotonics. 2014; 7:589–596. [PubMed: 23576407]

29. Sun Y, Liu R, Elson DS, Hollars CW, Jo JA, Park J, Sun Y, Marcu L. Simultaneous time-and wavelength-resolved fluorescence spectroscopy for near real-time tissue diagnosis. Opt. Lett. 2008; 33:630–632. [PubMed: 18347733]

30. Liu J, Sun Y, Qi J, Marcu L. A novel method for fast and robust estimation of fluorescence decay dynamics using constrained least-squares deconvolution with Laguerre expansion. Phys. Med. Biol. 2012; 57:843–865. [PubMed: 22290334]

31. Štefl M, James NG, Ross JA, Jameson DM. Applications of phasors to in vitro time-resolved fluorescence measurements. Analytical biochemistry. 2011; 410:62–69. [PubMed: 21078290]

32. Fereidouni F, Bader AN, Gerritsen HC. Spectral phasor analysis allows rapid and reliable unmixing of fluorescence microscopy spectral images. Optics express. 2012; 20:12729–12741. [PubMed: 22714302]

33. Andrews LM, Jones MR, Digman MA, Gratton E. Spectral phasor analysis of Pyronin Y labeled RNA microenvironments in living cells. Biomedical optics express. 2013; 4:171–177. [PubMed: 23304656]

34. Leray A, Spriet C, Trinel D, Usson Y, Héliot L. Generalization of the polar representation in time domain fluorescence lifetime imaging microscopy for biological applications: practical implementation. Journal of microscopy. 2012; 248:66–76. [PubMed: 22971219]

35. Pande P, Jo JA. Automated Analysis of Fluorescence Lifetime Imaging Microscopy (FLIM) Data Based on the Laguerre Deconvolution Method. IEEE transactions on bio-medical engineering. 2011; 58:172–181. [PubMed: 20934946]

36. Zhang Y, Chen Y, Li DD-U. Optimizing Laguerre expansion based deconvolution methods for analysing bi-exponential fluorescence lifetime images. Optics express. 2016; 24:13894–13905. [PubMed: 27410552]

37. Marcu L, , French PM, , Elson DS. Fluorescence lifetime spectroscopy and imaging: principles and applications in biomedical diagnostics CRC Press; 2014

38. Ma D, Liu J, Qi J, Marcu L. Reply to Comment:'A novel method for fast and robust estimation of fluorescence decay dynamics using constrained least-square deconvolution with Laguerre expansion'. Physics in Medicine and Biology. 2017; 62:1637. [PubMed: 28145280]

39. Reinhart GD, Marzola P, Jameson DM, Gratton E. A method for on-line background subtraction in frequency domain fluorometry. Journal of fluorescence. 1991; 1:153–162. [PubMed: 24242993]

40. Yankelevich DR, Ma D, Liu J, Sun Y, Sun Y, Bec J, Elson DS, Marcu L. Design and evaluation of a device for fast multispectral time-resolved fluorescence spectroscopy and imaging. Review of Scientific Instruments. 2014; 85:034303. [PubMed: 24689603]

41. Pal H, Nad S, Kumbhakar M. Photophysical properties of coumarin-120: unusual behavior in nonpolar solvents. The Journal of chemical physics. 2003; 119:443–452.

42. O'Connor D, Ware W, Andre J. Deconvolution of fluorescence decay curves. A critical comparison of techniques. Journal of Physical Chemistry. 1979; 83:1333–1343.
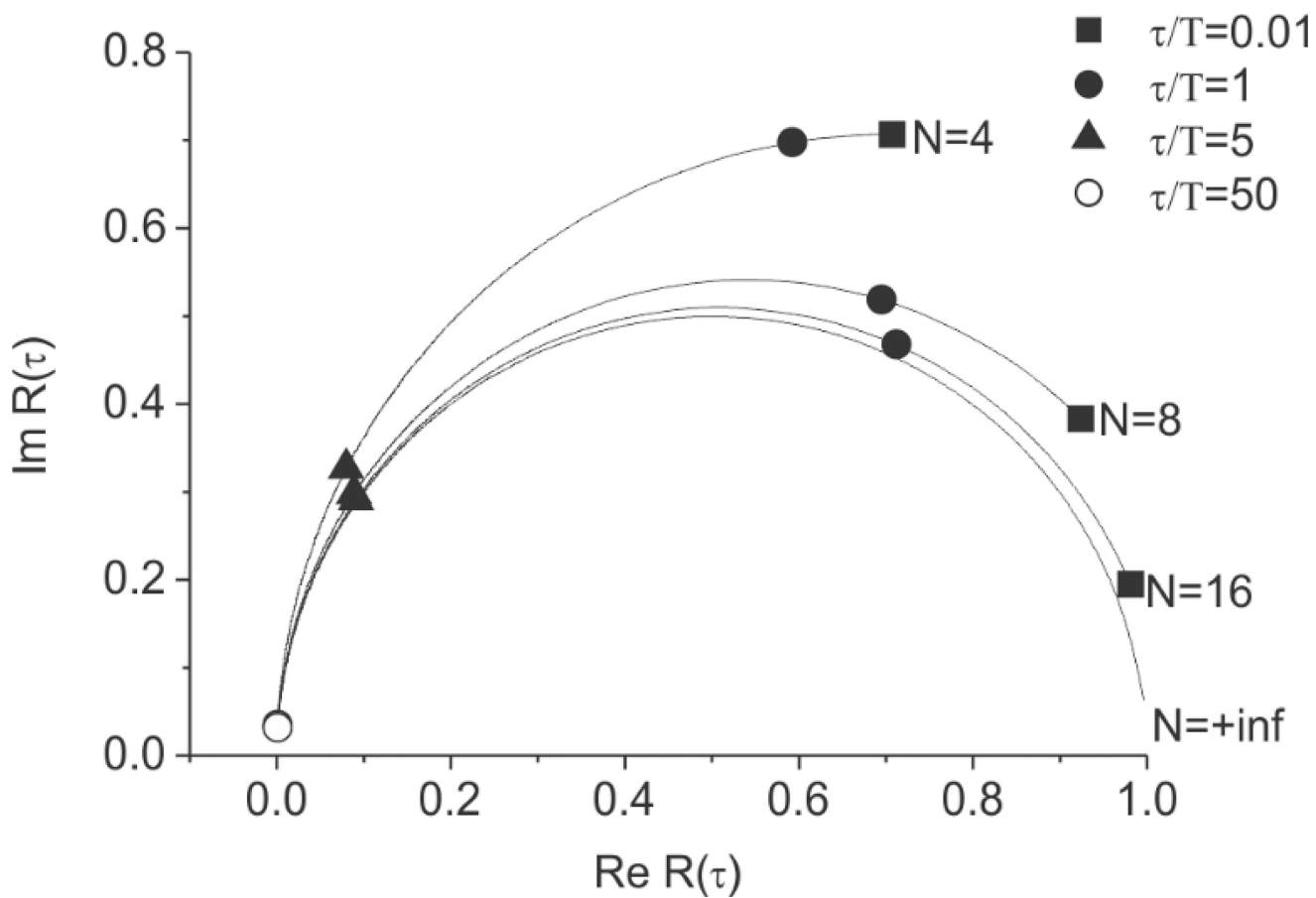
Figure 1.
Plot of the modified semi-circle for different number of sampling points
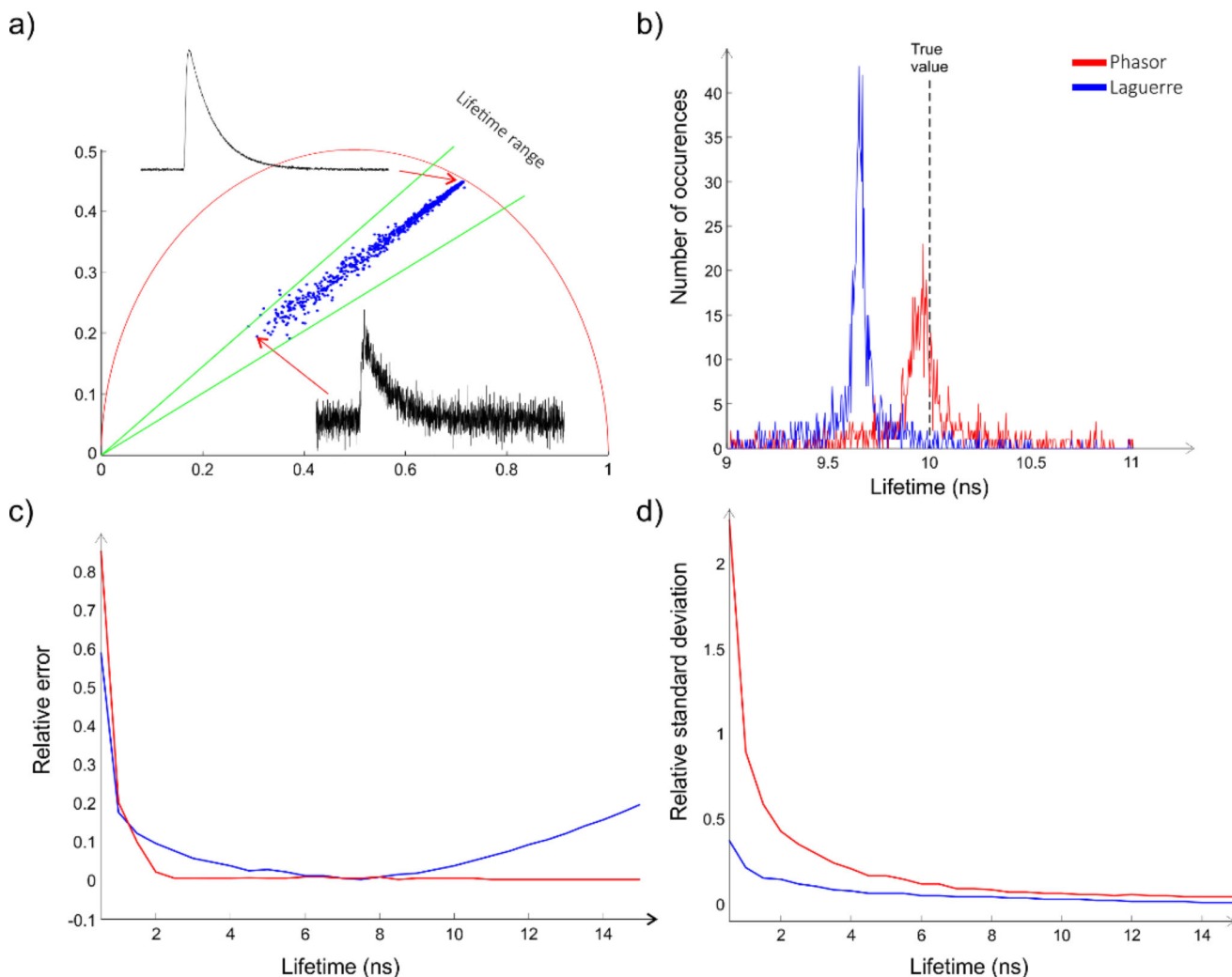
Figure 2.
(a) The phasor plot for decay curves with given lifetime of 10 ns and different noise level. As the SNR decreases the phasor points are shifted towards the origin of the graph. (b) Histograms of lifetime estimation from phasor and Laguerre method. Phasor shows broader distribution but more accurate results. (c) The relative error for lifetimes from 0.5 ns to 10 ns calculated with both methods. (d) Relative standard deviation for same lifetime range as in (c) for whole range of SNRs from 10 dB to 60 dB.
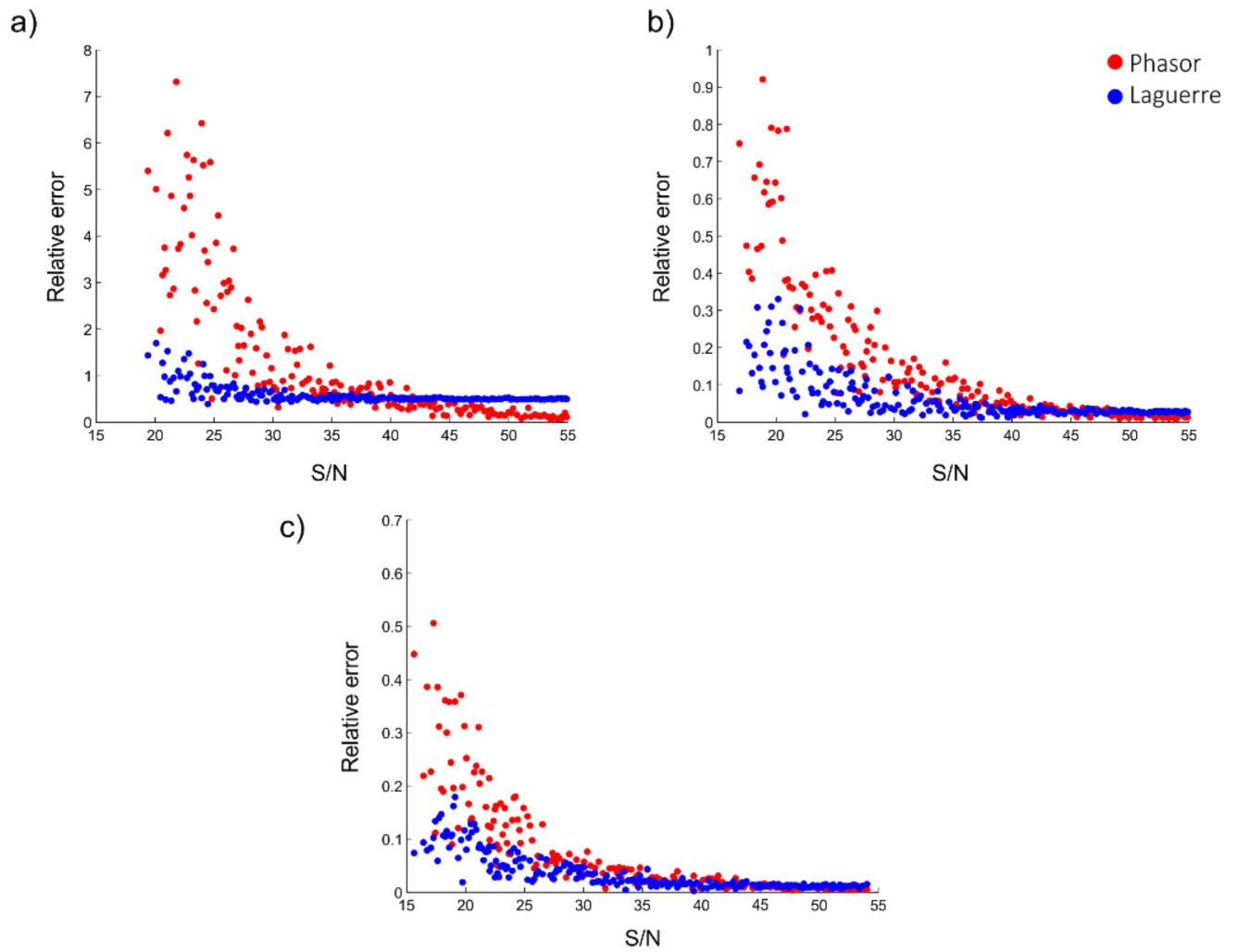
Figure (3).
The relative error as a function of SNR for different lifetimes (a)1 ns (b)5 ns (c)10 ns and with Gaussian noise calculated by phasor and Laguerre method.
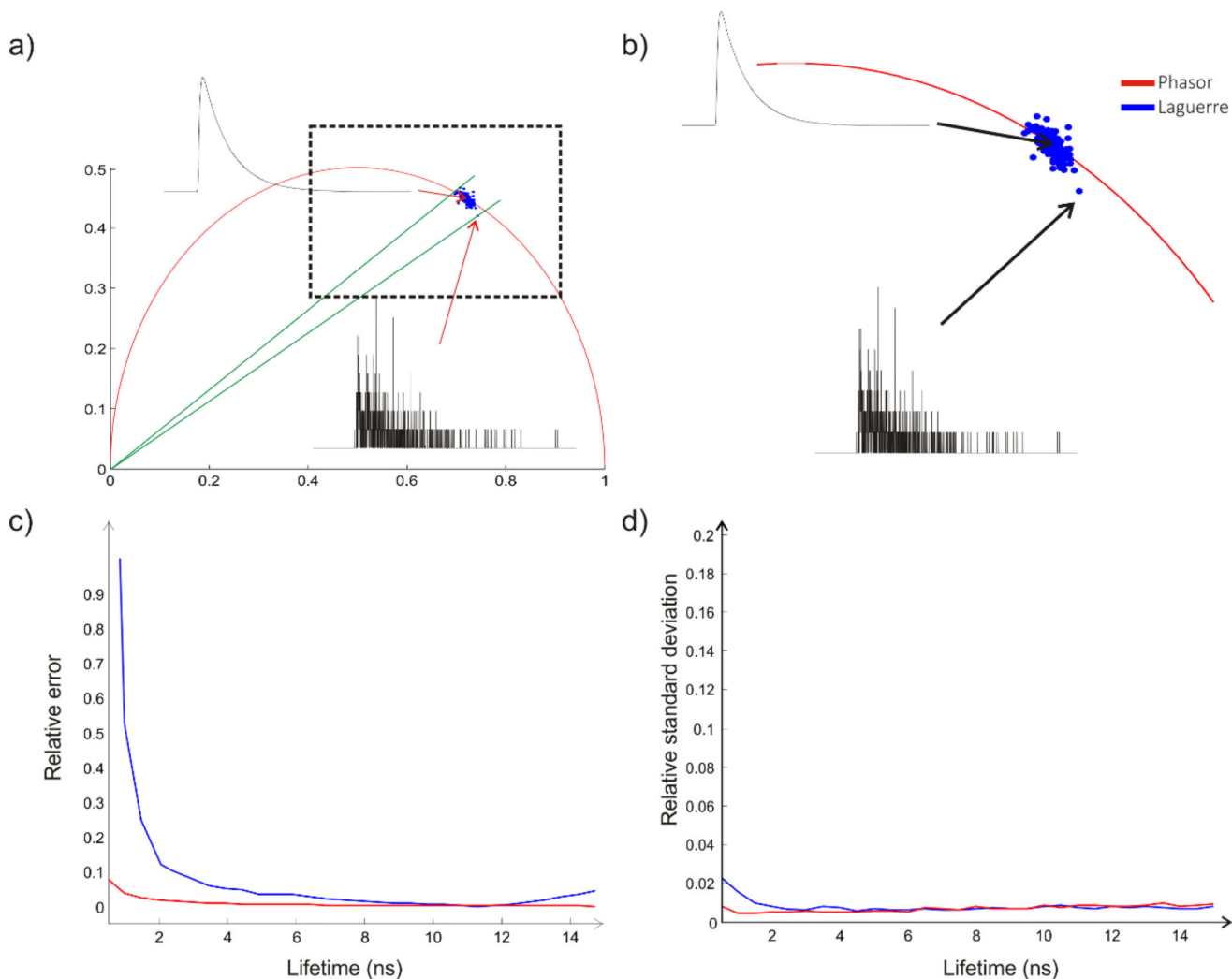
Figure 4.
(a) The phasor plot for decay curves with given lifetime of 10 ns and different Poissonian noise levels. As the SNR decreases the phasor points become more scattered around the given phasor point. (b) Zoomed in region from (a). (c) The relative error for lifetimes from 0.5 ns to 10 ns calculated with both methods. (d) Relative standard deviation for same lifetime range as in (c).
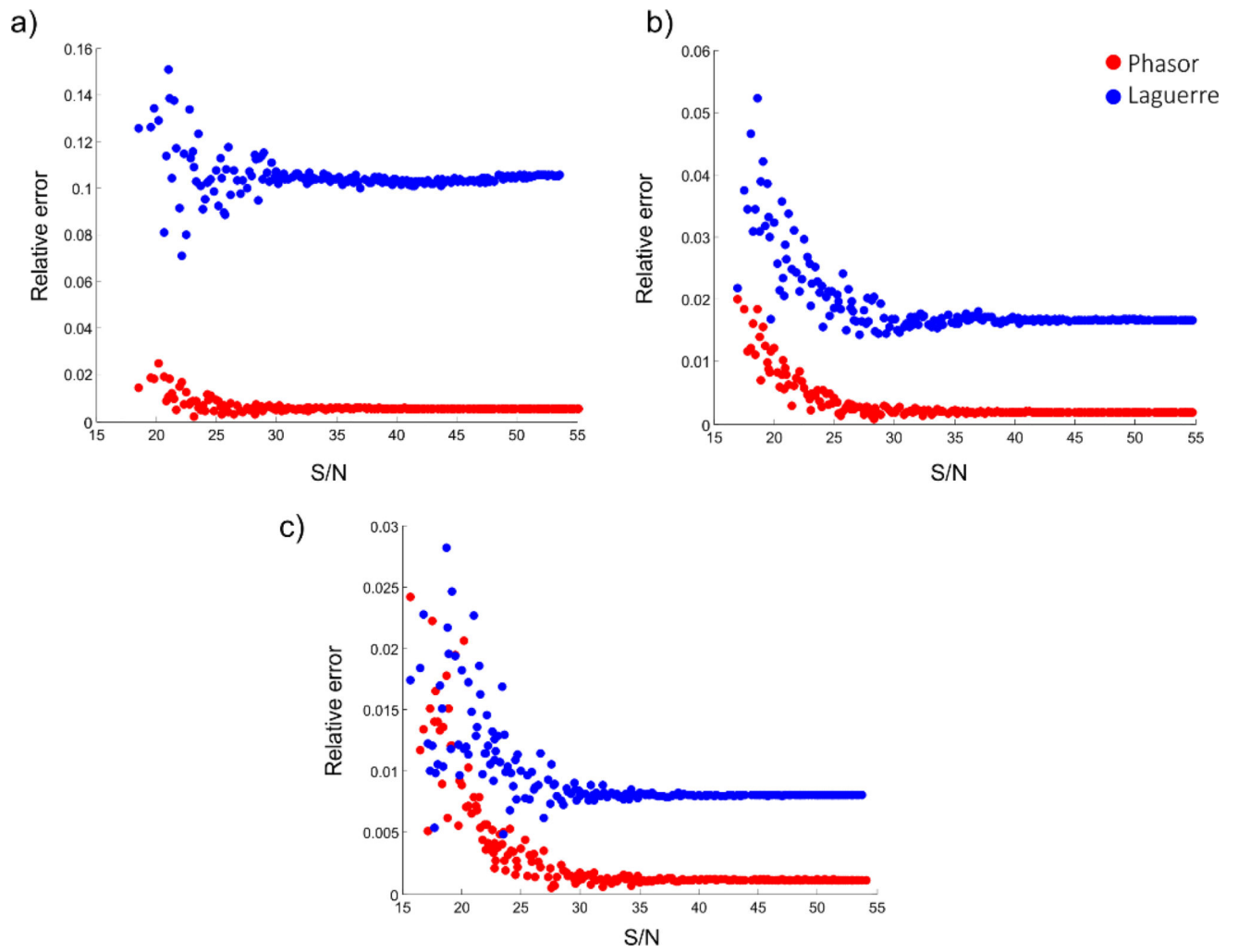
Figure 5.
The relative error as a function of SNR for different lifetimes (a)1 ns (b)5 ns (c)10 ns and with Poissonian noise calculated by phasor and Laguerre method.
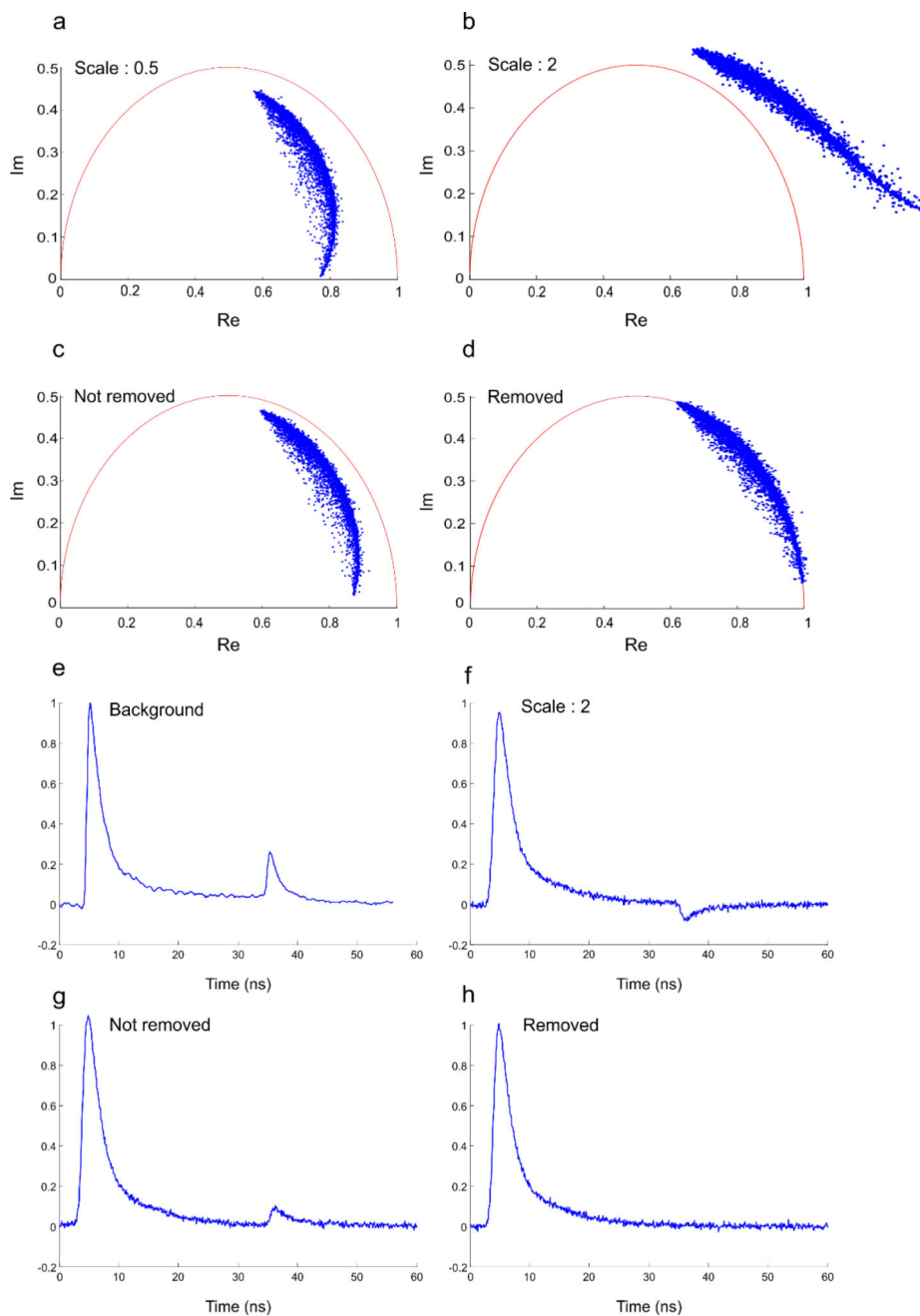
Figure 6.
Phasor plots for different background treatments. (a) background removed with scaling factor of 0.5. This causes the phasor points to move towards the origin of the semicircle. (b) background is subtracted with scaling factor of 2 where it pushes the phasor points outside of the semicircle. The artefact is more obvious with shorter lifetime values. (c) background is not removed and (d) background is properly removed. (e) measured background signal, (f)example of a decay curve where background is subtracted with scaling factor of 2.(g) background is not removed and (h) background is removed.
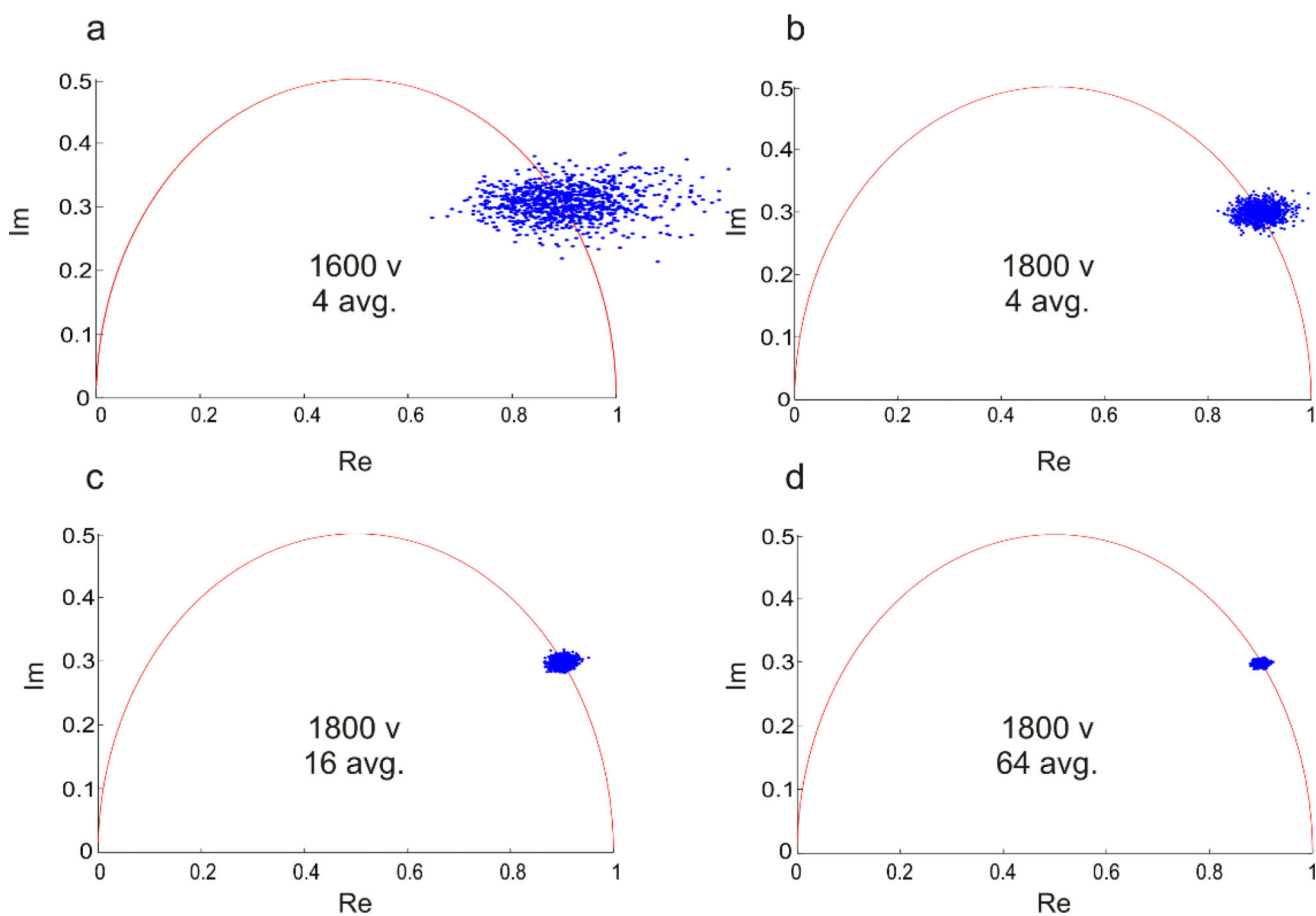
Figure 7.
The phasor plot for fluorescence decay curves of Coumarin solution recorded with 4 different PMT voltages and averaging (a) 1600V and 4 averages (b) 1800V and 4 averages (c) 1800V and 16 averages (d) 1800V and 64 averages.
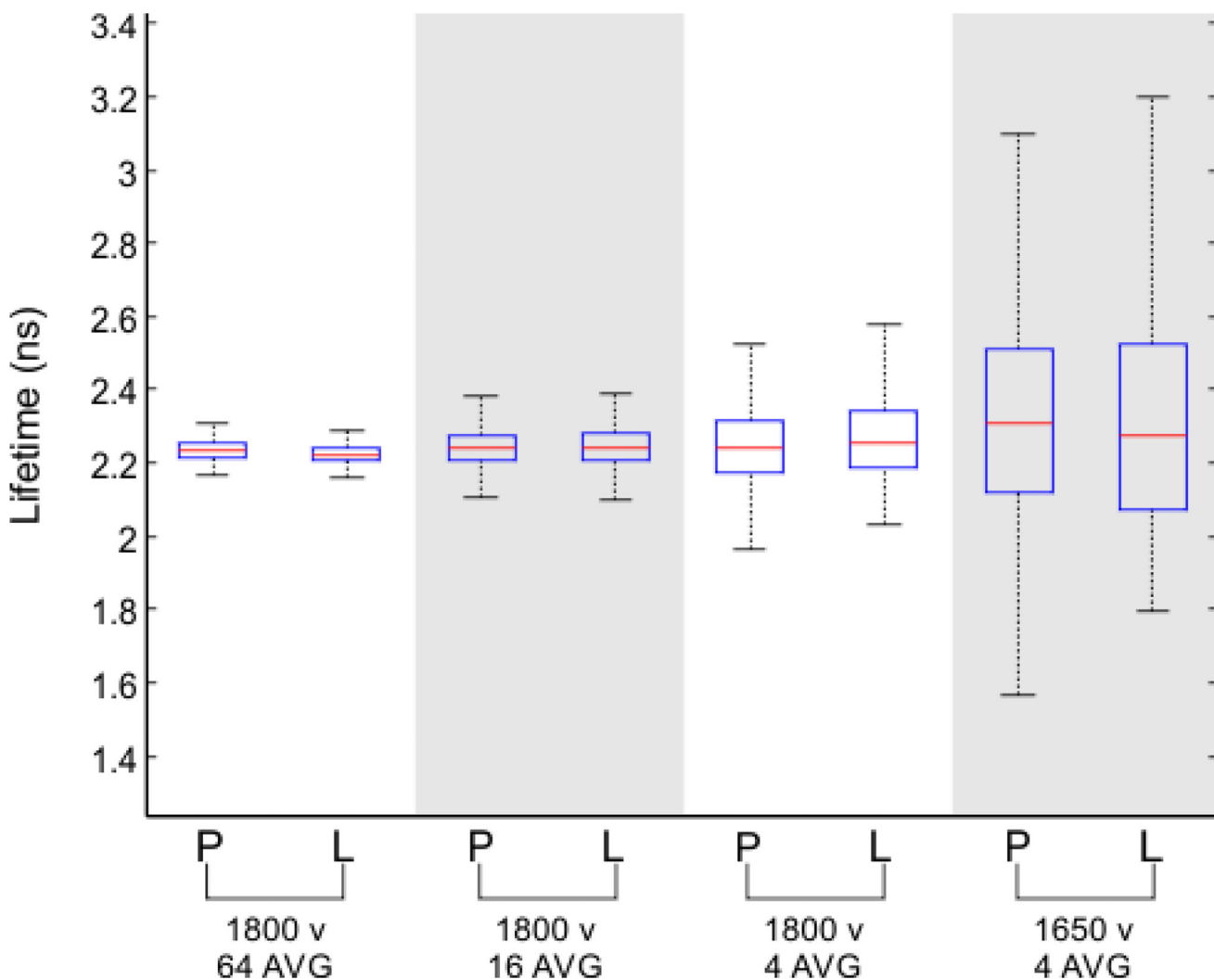
Figure 8.
Box plot for 4 different settings of PMT voltage and averaging size. P stands for phasor and L for Laguerre. The top and bottom of each "box" correspond the 25th and 75th percentiles of the lifetime distribution. The medians of lifetime measurements are shown in the middle of each box with a red line. The whiskers depict the extent of the data.
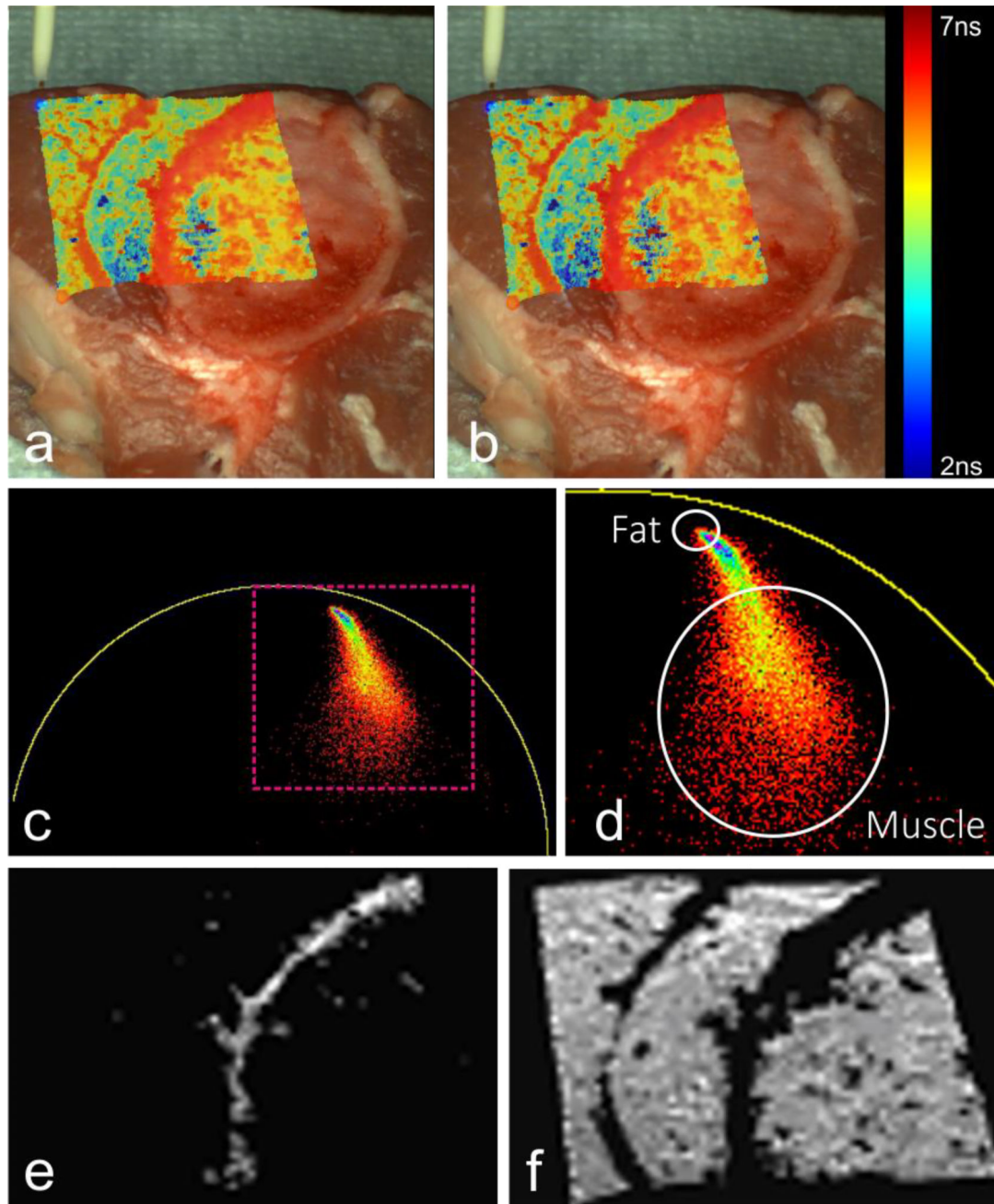
Figure 9.
Lifetime image of lamb tissue analyzed with (a) phasor and (b) Laguerre (c) phasor transformation of the lifetime image, (d) zoomed region of the phasor plot (e) segmented fat tissue using the reciprocal property of the phasor (f) segmented muscle and bone marrow. Note that the bone is excluded from the highlighted region.

Table 1

Lifetime estimation results from phasor and Laguerre for simulated bi-exponential decay curves treated with different level of background scaling. Phasor method shows more susceptibility to background contribution in the decay curve, but when it subtracted properly from the decay curve, it shows lower relative error.

Simulation	Relative Error (Laguerre)	Relative Error (phasor)
Scaling 2	0.14	0.21
Scaling 0.5	0.06	0.22
Properly removed	0.06	0.04
Not removed	0.07	0.2